Electromechanical engineering project

Authors:

REKIEK Saad

SWALUS Nick

TORABI Aryan
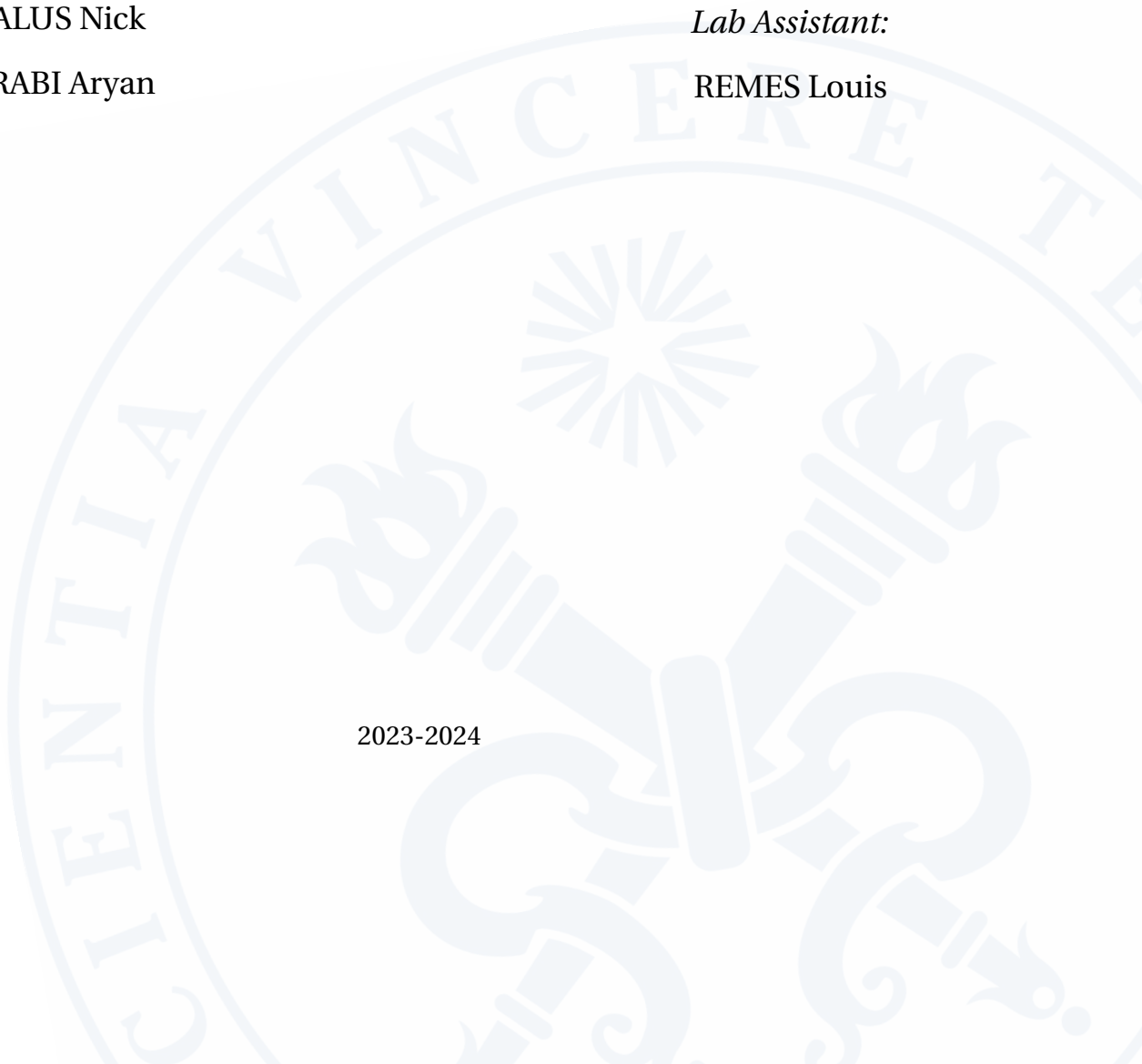
Lab responsible:

BERKE Peter

Lab Assistant:

REMES Louis

2023-2024

Contents

Introduction

The finite element (FE) method is a computational tool used to solve problems governed by partial differential equations. In this project, it is applied to linear solid mechanics. The project was performed in mixed ULB-VUB-International groups of three students. The project work served as a practical illustration of the main concepts in the field of FE-modelling, in order to provide a deep understanding of the theoretical concepts of the method by their practical implementation into a FE code and to offer a first experience using a finite element software employed in the industry (pre-processing, analysis, post-processing). [BR23b]

During six on campus sessions of four hours and many hours of work at home, the main goal was to quantify the axial and rotational stiffness of an engine mount via linear elastic finite element modelling [BR23a]. To get a sense of how finite element modelling works in practice, a Matlab code program was completed and verified during the first sessions of the project. Therefore, multiple concepts which were discussed in the theory classes were applied. Afterwards, a finite element model of the engine mount was created using Salome-Meca. In this way, its axial and rotational stiffnesses were determined for a simple and an advanced model, which results were compared subsequently. Finally, using a simple plate model, a convergence study was done to show equivalence between the Salome-Meca results and the analytical, closed form solution. All of the explained topics will be discussed in the continuation of this project report.

Part I

Project assignment

FE Model Setup

1.1 Model Abstraction

During this project, one used the engine mount made of steel. The part is shown in figure 6.1. As can be seen, the wider end of the part, which is normally connected to the engine, contains a lot of rubber in order to dampen its vibrations. However, the other side of the part only contains a very small layer of rubber. This contribution to the vibration damping can be neglected, as well as the steel which has a much higher stiffness. Therefore, one only took the wider rubber part into account for our model.

1.2 Geometry, Properties and Loads

At first sight, the rubber part has a basic circular shape. When one looks closely, one can see that the rubber part is not a full circle, but that only a cross connects the engine mount to the engine. Therefore, for the simplified model, a perforated cylinder of rubber was used, while one took a design of the rubber cross shape for the advanced model with the centre piece made of steel. In both models, one used a Young's modulus of 0.1 GPa and a Poisson's ratio of 0.5 for the rubber and 210 GPA and 0.28 for the steel.

For the simplified model, axial loads of 1000N are applied on both sides of the cylinder in the same perpendicular direction as well as on half of the inner circle to simulate the vibrations and the weight of the engine connected inside the hole (steel part not taken into account) with boundary conditions being the outer face of the cylinder. For the advanced model, the axial loads are applied on both faces of the steel centre piece in the same direction, as well as on half of the inner circle as explained earlier. Here, the boundary conditions are the 4 outer faces of the rubber cross. The results of the axial load simulations of both models can be seen on figure 6.2 and figure 6.3.

For the rotational loads, one applied nearly the same loads on both models. The only difference was that the loads on both faces were now oriented in the opposite directions perpendicular to the faces, so that a combination with the load on half of the inner circle would result in a rotation. In this way, one applied a load of 500N (and -500N) on both faces and 1000N on the inner circle. The results of the rotational load simulations can be seen on figure 6.4 and figure 6.5.

1.3   Mesh

The type of elements and the size of each element can theoretically be chosen freely. Nevertheless, there are a few things to keep in mind. In the end, one should be able to compare the results obtained in Salome-Meca with the results obtained by using the Matlab code. As the latter is only designed to use tetrahedral first order elements, the same element type should be used when creating a mesh in Salome-Meca. Additionally, the the size of the elements are important as well. Smaller but more elements at stressed or complex locations (mesh refinement) would result in a better approximation of the shape of the model and a more precise stress distribution inside the model.

To show the importance of the mesh refinement, one conducted a convergence test. One applied an axial load of 1 kN on the previously mentioned faces and one obtained the convergence graphs shown in figure 6.6 and figure 6.7. Both graphs are acquired by changing number of nodes by decreasing the mesh size for both simplified and advanced models. One can conclude that the stress will increase slowly for both models. At a certain point, if you keep increasing the number of nodes, one wouldn't notice any difference anymore. For the advanced model, this is approximately the case. For the simple model, the value keeps increasing and is not stabilising, so can conclude that the simple model is not accurate to get to a valid solution.

1.4   Assumptions and simplifications

In order to be able to execute our model simulations in a limited time, one applied a few assumptions and simplifications. These are used to make our models and tests easier, but it is important to ensure that the results still remain representative for the real life situation. Some of the assumptions and simplifications one made are explained in the following list:

- As explained earlier, only the big rubber part on the wider end of the engine mount was taken

into account for our models. The other side of the part only contains a very small layer of rubber which will nearly contribute to the vibration damping. The deformation of the steel part of the engine mount can be neglected as well seen the much higher Young's Modulus compared to rubber.

- The applied loads in our simulations only represent the vibration forces created by the moving pistons inside the engine of the car. When driving a car, there are many other vibration sources which can create additional loads on the car and so on the engine mount. All of these other sources were neglected during this project.

- For our simulations in Salome-Meca, first order tetrahedral elements were used. This was done because one had to compare the results obtained with Salome-Meca with the ones from the Matlab code in the end. Seen that the Matlab code is only designed for this type of elements, it needed to be used in Salome-Meca as well. This creates a small deviation compared to the results which can be obtained by using higher order elements and which would result in a more accurate solution.

- Seen that one uses a linear code, linear displacements and linear materials, the complexity of the project problem is significantly reduced. In real life, there are many non-linearities to take into account. In addition, a material is never perfectly uniform distributed and damage, cracks, etc. will have a huge impact on the behaviour of a material.

Numerical Results

The following formula [Omn23] was used in order to calculate the axial stiffnesses of the simple and the advanced models when one applies an axial loading as explained in chapter 1:

$$k_{\text{axial}} = F_{\text{load}}/q \tag{2.1}$$

To calculate the rotational stiffnesses, one applied the equivalent formula for rotation [Omn23]:

$$k_{\text{rotational}} = M_{\text{load}}/\theta \tag{2.2}$$

2.1 Simple Model

As explained earlier in this report, the rubber will deform the most and will result in the largest displacements within the part. Therefore, the steel part was not included in our simple model. Using the applied loads on the corresponding surfaces as discussed in chapter 1, the axial stiffness for the simple model is equal to 125 kN/m and the rotational stiffness is equal to 37.03 kNm/rad.

2.2 Advanced Model

For the advanced model, the centre steel part of the cross was taken into account in order to be able to connect the rubber parts all together. Using the same loads as also explained in chapter 1, the axial stiffness is equal to 1388.88 kN/m and the rotational stiffness equals 217.39 Nm/rad.

3

Discussion on the results

The influence of modelling assumptions on the numerical outcomes and their alignment with real-world behaviour is considerable in this project. Simplifying the engine support's geometry and material properties might make the results deviating from how the component behaves in real life. Ignoring parts assumed to have minimal deformation could lead to missing actual structural responses. Assumptions about material properties and geometric features, like the substantial Young's modulus difference between rubber and steel, could introduce inaccuracies. This might underestimate steel deformations compared to rubber, impacting the overall stiffness analysis. Additionally, the choice for a first order tetrahedral element computation can introduce errors in stress and strain calculations due to inherent precision limitations. Efforts to mirror real-world loading conditions might simplify boundary conditions and load distributions as well, potentially impacting result accuracy. It shouldn't be surprising that the advanced model simulations resulted in much more accurate solutions than the simple model did.

How can we improve the model?

A finer mesh can yield more precise results, capturing localised effects but demanding more computational resources. One could also make a more advanced podel of the engine mount, taking into account every detail. An other option is to use advanced methods like non-linear or dynamic analysis to understand complex behaviours such as material non-linearities, dynamic responses, or fluid-structure interactions. Furthermore, one could validate the model while comparing it to experimental data to ensure accuracy and reliability. Finally, one could adjust the model parameters to match real-world observations and imperfections of a material.

4

Conclusions

The computational findings from this project, revealing insights into the axial and rotational stiffness of the engine mount, underscore the impact of modelling assumptions on numerical predictions. The implementation of the Finite Element Method (FEM) facilitated the estimation of stresses, strains and deformations, allowing a fundamental grasp of the structural behaviour under specific loads. However, these outcomes hinge on diverse modelling assumptions, encompassing geometric simplifications, material abstractions, and chosen mesh setups. The simplifications, which are crucial for computational feasibility, might not fully capture the nuanced behaviour of the actual mechanical part.

From an educational standpoint, this project shed a light on the trade-offs between model intricacy and computational efficiency. It emphasised the need to critically use modelling assumptions and their impact on simulation accuracy. The observed differences between the simulations and the real-world behaviour stress the importance of cautiously interpreting computational results and validating models against real data. Moreover, this project served as a platform for refining modelling techniques, understanding the significance of material properties, and acknowledging the role of boundary conditions in computational analysis. The experience gained from this gave us valuable insights into the challenges and intricacies of translating real-world engineering problems into computationally solvable models. Ultimately, while the computational results offer a fundamental comprehension of the system's behaviour, their limitations underscore the ongoing necessity to refine models and validate outcomes against empirical observations. This validation ensures their applicability and reliability in practical engineering scenarios.

5

References

In this chapter, the list of references one used during the project is presented:

- Young's Modulus: [The03]

- Poisson's Ratio: [The08]

- Stiffness formulas: [Omn23]

- Stress concentration factor formula: [Ame05]

Figure and tables

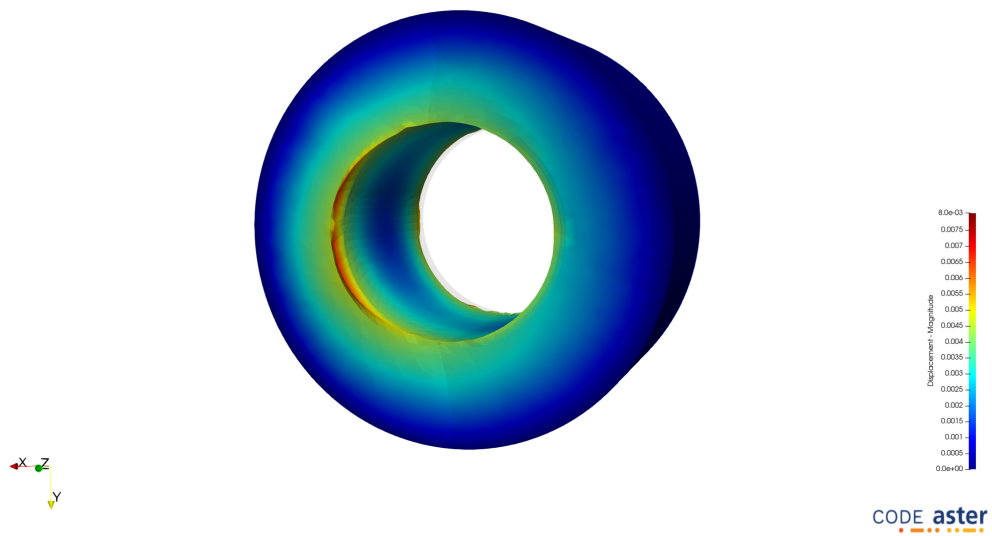Figure 6.1: Picture of the engine mount

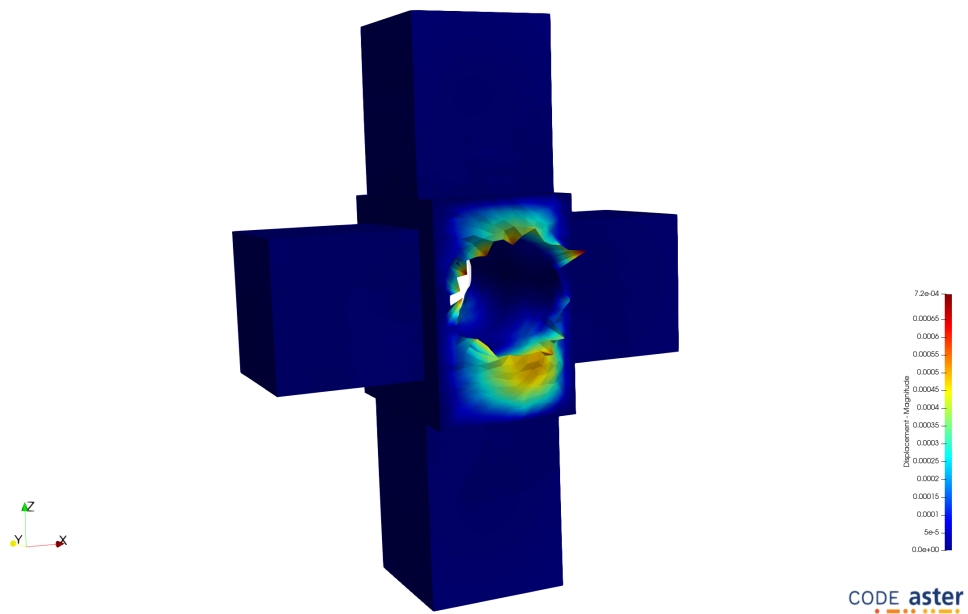Figure 6.2: Simple model with axial loads

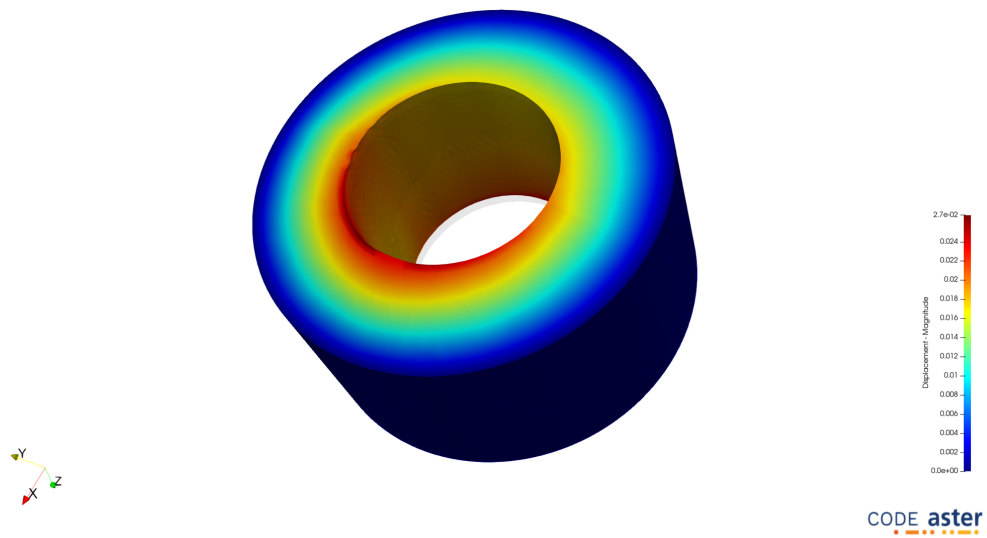Figure 6.3: Advanced model with axial loads
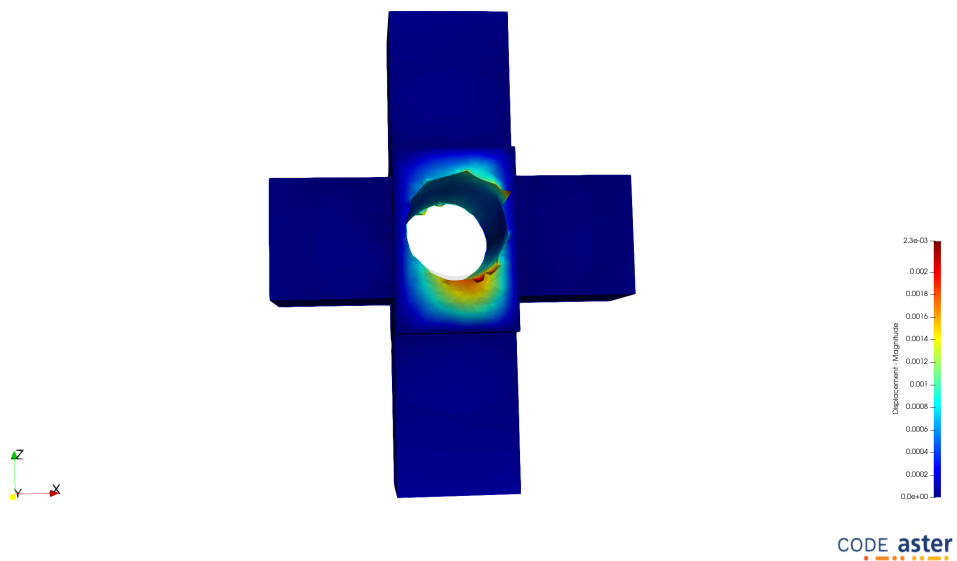
Figure 6.4: Simple model with rotational loads
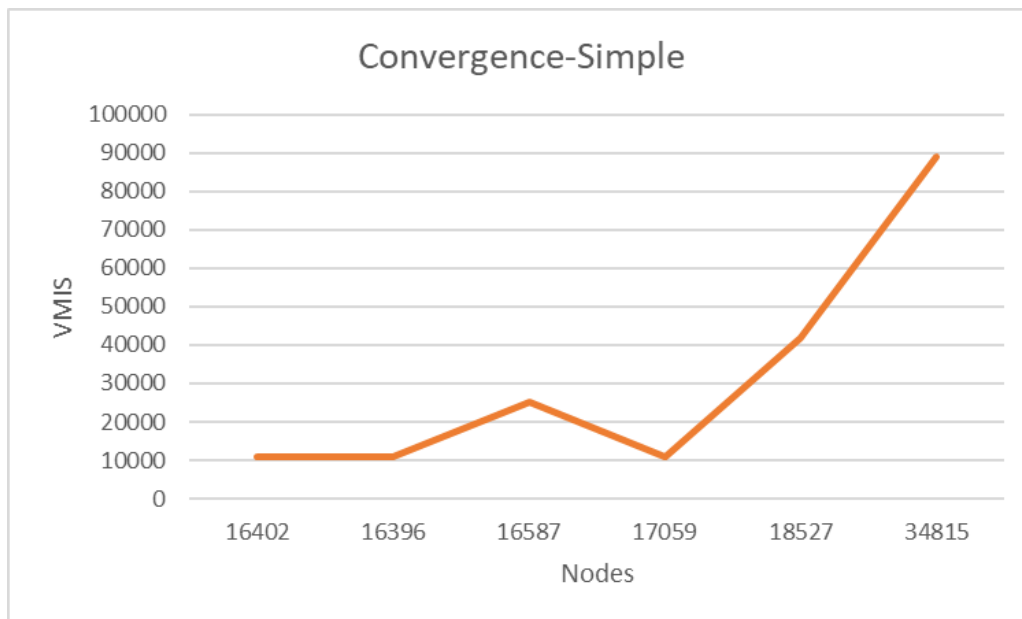

Figure 6.5: Advanced model with rotational loads
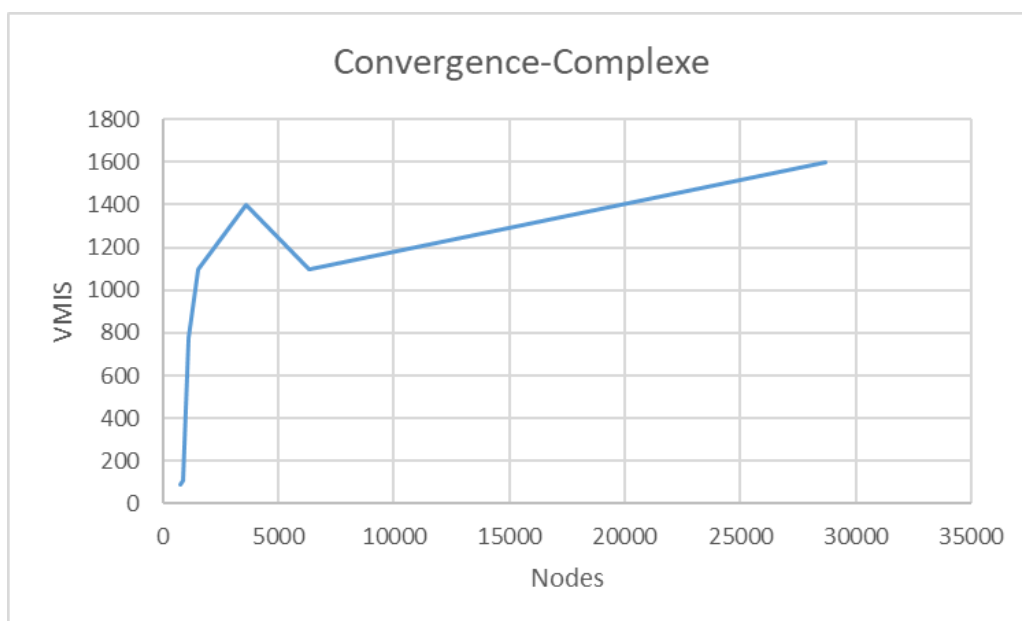
Figure 6.6: Convergence check for the simple model

Figure 6.7: Convergence check for the advanced model

Part II

Matlab implementation

7

FE Code Verification

7.1 Single element

The single tetrahedral element was defined as follows: one node was placed in the origin of the coordinate system, while the other 3 nodes were located on each of the 3 axes at a distance of 1 from the origin. In each test, the following values are assumed: E = 1000, $\mu = 0.3$.

7.1.1 Tensile test

The tensile test done by displacing the node on the x-axis, y-axis and z-axis 1 unit along its axis direction. One expects normal stresses to be present in all three directions, with the values matching the following stress-strain relationship (similar in the y- and z-direction): $\epsilon_x = \frac{1}{E}(\sigma_x - \nu(\sigma_y + \sigma_z))$. Strain should only appear in the pulled direction with a value of 1 and there should be no shear stresses. The result of the tensile test of the node on the x-axis can be seen in table 7.1. The same test was also executed in the other two directions and one obtained the expected results.

ϵ_x, σ_x	ϵ_y, σ_y	ϵ_z, σ_z	γ_{xy}, τ_{xy}	γ_{xz}, τ_{xz}	γ_{yz}, τ_{yz}
1	0	0	0	0	0
1346.2	576.9	576.9	0	0	0

Table 7.1: Strains and stresses for the tensile test in the x-direction (single element)

7.1.2 Shear test

The shear tests are executed by applying a displacement of a node in an other direction than the axis it is located on. Shear stresses and strains are only expected in the plane determined by the node and the pulled direction. The shear strain should be equal to the displacement, while the value of the shear stress should match the definition of the shear modulus (similar in the yz- and xz-plane): $\tau_{xy} = G\gamma_{xy}$ with $G = \frac{E}{2(1+\nu)}$.

The results of a unitary displacement of the x-node in the y-direction can be found in table 7.2. The same test was also executed in the other two planes and one obtained the expected results.

ϵ_x, σ_x	ϵ_y, σ_y	ϵ_z, σ_z	γ_{xy}, τ_{xy}	γ_{xz}, τ_{xz}	γ_{yz}, τ_{yz}
0	0	0	1	0	0
0	0	0	384.61	0	0

Table 7.2: Strains and stresses for the shear test of the x-node in the y-direction (single element)

7.1.3   Rigid body translation test

The rigid body translation tests for the single element are executed by applying a displacement of all nodes in the same direction. One doesn't expect any strains or stresses. A rigid body translation of 1 unit in the x-direction was performed and, as expected, there were no stresses or strains created. The same test was also executed in the other two directions and one obtained the same results.

7.1.4   Rigid body rotation test

For the rigid body rotation tests, the element was rotated around each of the 3 axes. Each time, the 2 nodes on the rotation axis were fixed, while a displacement was applied on the other 2 nodes. As one assumes very small rotations in the final structure, the displacement around the circle could be approximated to be perpendicular to the axis of the node. A counter-clockwise rotation test was performed around the x-axis. As expected, no stresses or strains were created. The same test was also executed around the other 2 axes and one obtained the same results.

7.2   Cube consisting of 12 elements

Once the single element was verified, it was necessary to validate an assembly of multiple elements. Therefore, a single cube was used, which consisted of 12 tetrahedral elements. Eight nodes were defined by the corners of the cube, the ninth node was defined by the following coordinates: (0.4, 0.7, 0.6). The behaviour of this ninth node will be checked by applying displacements to the 8 corner nodes. Each test will be executed for both boundary conditions (direct and penalty method) and for the following values: E = 1000, μ = 0.3. For the penalty method, a Z-value of 10^7 was used.

7.2.1   Tensile test

A tensile test can be executed by applying a displacement of 0.1 to the 4 nodes defining a face of the cube in the direction perpendicular to the face. The other corner nodes and directions are fixed. One expects that the ninth node will make a displacement proportional to its coordinates and only in the direction of the displacement. One of the tests was a displacement of the face defined by nodes 2, 5, 6 and 8 in the x-direction. Proportional to the coordinates of the ninth node, one expected only a displacement of 0.04 units in the x-direction. As can be seen in table 7.3, this was indeed the case for both boundary conditions. The test was repeated on the other faces and resulted in the same proportional displacement (0.07 and 0.06 units).

Tensile test	Method	x-direction	y-direction	z-direction
X-direction	Direct	0.04	0	0
	Penalty	0.04	-7.05e-07	-3.70e-07

Table 7.3: Displacements of the ninth node for a tensile test in the x-direction

7.2.2   Shear test

For a shear test, a displacement of 0.1 should be applied on all 6 nodes of two adjacent faces of the cube, perpendicular to the test plane. The direction of the displacements should be defined towards the common edge of the faces. All other nodes and directions are fixed. For example, in the case of a shear test in the xy-plane, nodes 3, 5, 7 and 8 should have a displacement in the x-direction and nodes 2, 5, 6 and 8 in the y-direction. The results of this test can be seen in table 7.4. As expected, the ninth node displacements only appear in the x- and y-directions and are proportional to the opposite coordinate of the ninth node. This test was repeated for the other planes and resulted in the same proportional displacements.

Shear test	Method	x-direction	y-direction	z-direction
xy-plane	Direct	0.07	0.04	0
	Penalty	0.07	0.04	1.17e-11

Table 7.4: Displacements of the ninth node for a shear test in the xy-plane

7.2.3   Rigid body translation test

The rigid body translation tests for the cube are executed by applying a displacement of all 8 nodes in the same direction. One expects an equal displacement of the ninth node in this direction. A rigid body translation of 0.1 in the x-direction was performed (for both boundary conditions) and,

as expected, the displacement of the ninth node in the x-direction was equal to 0.1 and 0 (or nearly 0) in the other directions. The same test was also executed in the other two directions and obtained the same result.

7.2.4   Rigid body rotation test

Finally, for the rigid body rotation tests, the cube was rotated around each of the 3 axes. Each time, the 2 nodes on the rotation axis were fixed, while a displacement was applied on the other 6 nodes. As one assumes very small rotations in the final structure, the displacements around the circle could be approximated to be perpendicular to the axis for the adjacent nodes of the fixed edge. For the 2 opposite nodes, there should be a displacement contribution in both perpendicular directions. A counter-clockwise rotation test was performed around the x-axis. As expected, the ninth node displacements only appear in the y- and z-directions and are proportional to the opposite coordinate of the ninth node for both boundary conditions. The signs are depending on the direction of rotation. The same test was also executed around the other axes and one obtained the expected results.

7.3   Convergence study with Salome-Meca

A convergence study of a plate with a hole was done in order to check convergence of the Salome-Meca software with the closed form solutions. Because one will only apply a force in the x-direction, the plate can be considered as a 2D-plate and one only had to take in to account one quarter of the plate. This piece of the plate was defined by the following parameters: length L = 100 mm, width W = 50 mm. Symmetry conditions were applied on the left and bottom faces (all directions are locked except the y-direction for the left face and the x-direction for the bottom face). The hole was placed in the bottom-left corner and had a radius R = 10 mm. One pulled on the right side of the plate with a loading σ of 100 kPa in the x-direction and checked the peak value of the stress on the edge of the hole. For an equal mesh size of 6 mm, this value was equal to 290 MPa. For a refined mesh with a maximum size of 3 mm, the result is 280 Mpa, which can also be seen on the figure in appendix A. One compared these values to an analytical solution by using the following formula of the stress concentration factor [Ame05]: $K_t = 3 - 3.14\frac{R}{W} + 3.667(\frac{R}{W})^2 - 1.527(\frac{R}{W})^3$. For the given parameters, this stress concentration factor is equal to 2.72, so for a loading of 100 kPa, the peak stress value should be 272 MPa, which is very close to the result obtained with Salome-Meca. Due to software crashes, a finer mesh was not possible to obtain a closer approximation.
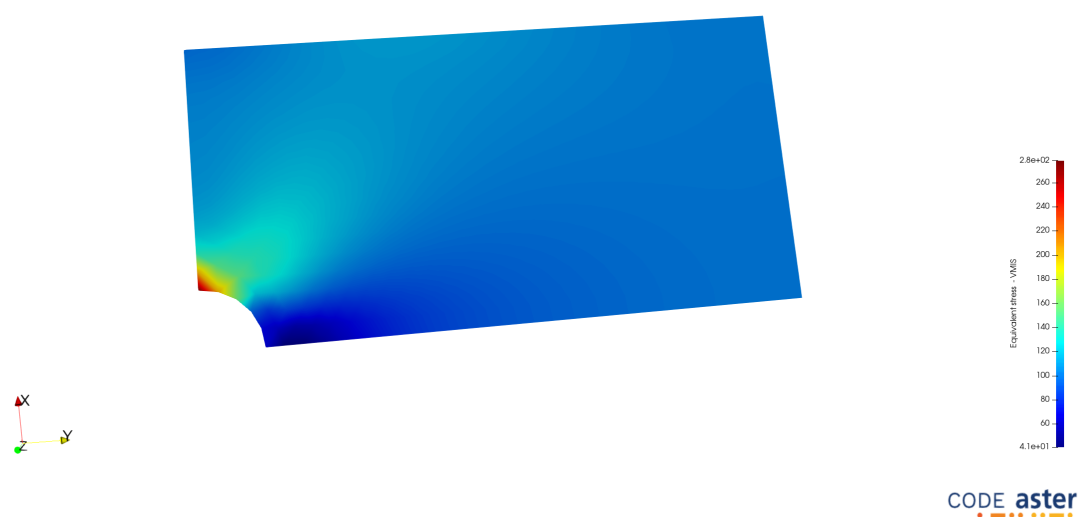
$\mathcal{A}$

Appendix

Figure A.1: Convergence test: Plate with a hole

Bibliography

[Ame05]   AmesWeb (2005). *Central single circular hole in finite-width plate*. URL: `https://amesweb.info/stress-concentration-factor-calculator/central-circular-hole-in-plate.aspx`. (accessed: 21.12.2023).

[BR23a]   Berke, P. and L. Remes (2023a). *Project assignment for the electromechanical engineering section*.

[BR23b]   Berke, Peter and Louis Remes (2023b). *Electromechanical engineering project task description*.

[Omn23]   Omni Calculator (2023). *Rotational Stiffness Calculator*. URL: `https://www.omnicalculator.com/physics/rotational-stiffness`. (accessed: 22.12.2023).

[The03]   The Engineering ToolBox (2003). *Young's Modulus, Tensile Strength and Yield Strength Values for some Materials*. URL: `https://www.engineeringtoolbox.com/young-modulus-d_417.html`. (accessed: 21.12.2023).

[The08]   —   (2008). *Poisson's Ratio*. URL: `https://www.engineeringtoolbox.com/poissons-ratio-d_1224.html`. (accessed: 21.12.2023).